Supporting Information

$LaSr_3NiRuO_4H_4$: a 4d transition-metal oxide-hydride containing metal hydride sheets.

Lun Jin, Michael Lane, Dihao Zeng, Franziska K. K. Kirschner, Franz Lang, Pascal Manuel, Stephen J. Blundell, John E. McGrady and Michael A. Hayward*

Table of Contents

7. Magnetic characterization of $LaSr_3NiRuO_4H_4$

Figure S5. Magnetisation of a $LaSr_3NiRuO_4H_4$ sample measured as a function of applied field at 300 K. A linear fit to high-field region (H > 20000 Oe) yields a gradient which is the paramagnetic susceptibility of the sample, and an intercept which is the saturated ferromagnetic moment of the sample.

8. μ^+SR experimental details

9. Computational details

Figure S6. $2\sqrt{2}$ x $2\sqrt{2}$ x 1 expanded unit cell used in the computational model. Grey: La; Brown: Sr; Green: Ni; Yellow: Ru; Red: O; Purple: H.

Figure S7. Structures, total energies and Ni/Ru DOS for the chequerboard, striped and double-striped arrangements of Ni/Ru in the unit cell.

Figure S8. DOS for the chequerboard structure, including H^- and O^{2-} DOS as well as Ru and Ni.

1. Synthesis of $LaSr_3NiRuO_8$

Samples of $LaSr_3NiRuO_8$ were prepared by a high-temperature ceramic method. Suitable stoichiometric ratios of La_2O_3 (99.999%, dried at 900°C), $SrCO_3$ (99.994%), RuO_2 (99.99%, dried at 800°C) and NiO (99.998%) were ground together using an agate mortar and pestle, transferred into an alumina crucible, and then heated at a rate of 1 ºC min^{-1} to 1000°C in air to decompose the carbonate. The sample was then reground, pressed into pellets and then heated for 3 periods of 48 hours at 1300°C in air, with grinding between heating periods.

2. Structural characterization of $LaSr_3NiRuO_8$.

Synchrotron X-ray powder diffraction data were collected from a sample of $LaSr_3NiRuO_8$, contained within a 0.3mm capillary, using the I11 diffractometer at the Diamond Light Source, UK. These data could be readily indexed using a body-centred tetragonal unit cell with lattice parameters: *a* = 3.89044(2) Å and *c* = 12.62974(7) Å, consistent with an *n* = 1 Ruddlesden-Popper structure. A structural model was constructed, based on an *n* = 1, A_2BO_4 Ruddlesden-Popper phase with a 1:3 La:Sr solid-solution on the A-site and a 1:1 Ni:Ru solid-solution on the B-site. This model was refined against the data to achieve a good statistical fit. A full description of the refined structural parameters is given in Table S1, with a plot of the observed and calculated data shown in Figure S1. Selected bond lengths are tabulated in Table S2.

	x	*y*	*z*	Fraction	U_{iso} (Å^2)
La/Sr(1)	0	0	0.35709(2)	0.25/0.75	0.0090(1)
Ni/Ru(1)	0	0	0	0.5/0.5	0.0040(2)
O(1)	0	0	0.1656(1)	1	0.0133(4)
O(2)	½	0	0	1	0.0060(6)
$LaSr_3NiRuO_8$ space group *I*4/*mmm* (#139) Formula weight : 689.53 g mol^{-1}, Z = 2 *a* = 3.8904(1) Å, *c* = 12.6297(1) Å, Volume = 191.16(1) Å^3					
Radiation source: Synchrotron X-ray, λ = 0.82626(1) Temperature: 298 K χ^2 = 9.87; *wRp* = 5.67 %; *Rp* = 3.63 %.					

Table S1. Structural parameters from the refinement $LaSr_3NiRuO_8$ against synchrotron X-ray powder diffraction data.

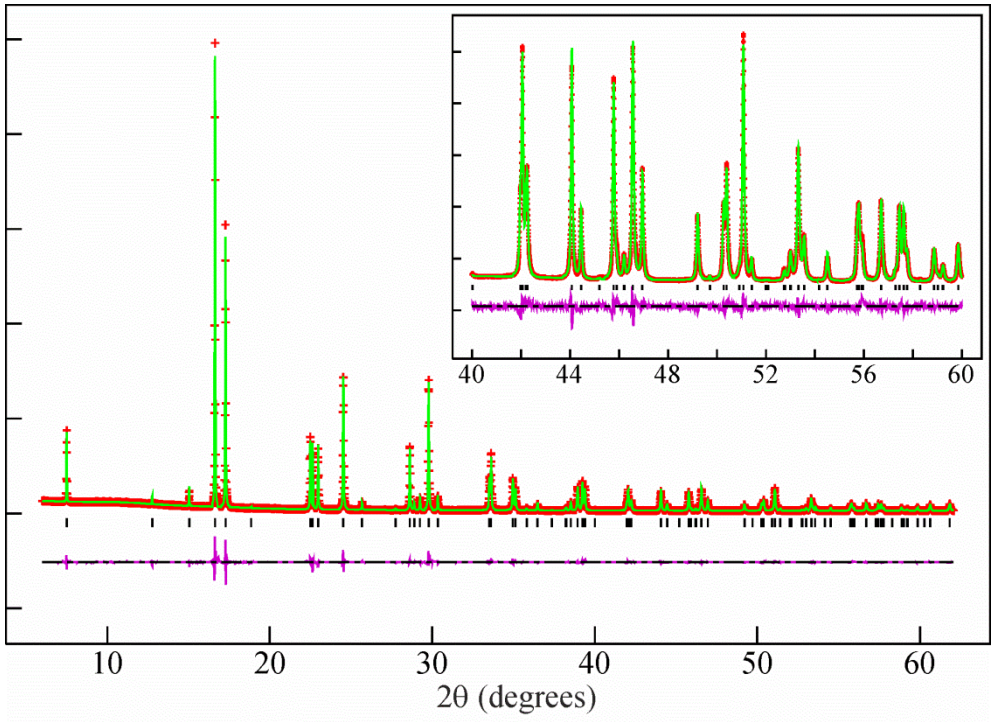

Figure S1. Observed, calculated and difference plots from the structural refinement of $LaSr_3NiRuO_8$ (space group *I*4/*mmm*) against synchrotron X-ray powder diffraction data collected at 300 K.

Cation	Anion	length (Å)
La/Sr(1)	O(1)	2.418(1) × 1
	O(1)	2.766(1) × 4
	O(2)	2.654(1) × 4
Ni/Ru(1)	O(1)	2.091(1) × 2
	O(2)	1.945(1) × 4

Table S2. Selected bond lengths from the refined structure of $LaSr_3NiRuO_8$.

3. Magnetic characterisation of $LaSr_3NiRuO_8$.

Zero-field-cooled and field-cooled magnetisation data collected from $LaSr_3NiRuO_8$ as a function of temperature in an applied field of 100 Oe, using a Quantum Design SQUID magnetometer, are shown in Figure S2. Data in the range 150 < T/K < 300 can be fitted to the Curie-Weiss law ($\chi = C/(T - \theta)$) to yield values of C = 2.73(1) cm^3 K mol^{-1}, θ = -91.5(2) K. The zero-field-cooled and field cooled data diverge below T = 55 K, consistent with the onset of canted antiferromagnetic order. Magnetisation data collected at 300 K as a function of applied field (Figure S3) are linear and pass through the origin. Analogous data collected at 5 K after cooling in an applied field of 50000 Oe exhibit hysteresis consistent with weak ferromagnetism.

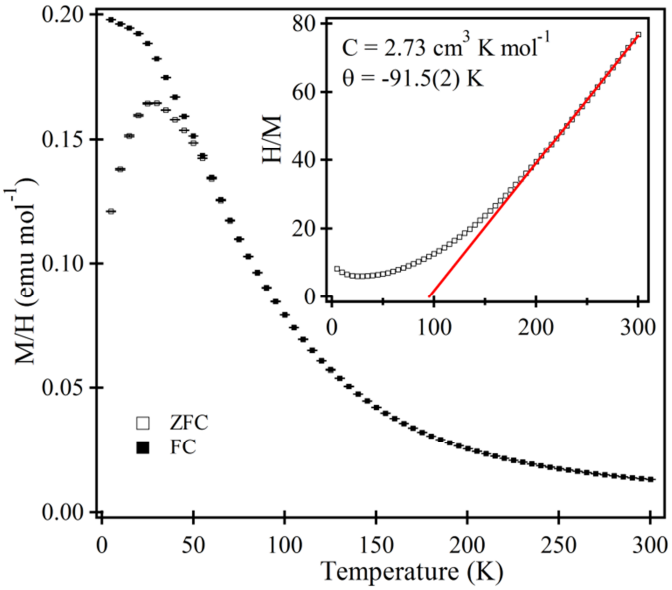

Figure S2. Zero-field-cooled and field-cooled magnetisation data collected from $LaSr_3NiRuO_8$ in an applied field of 100 Oe. Inset shows fit to the Curie-Weiss law.

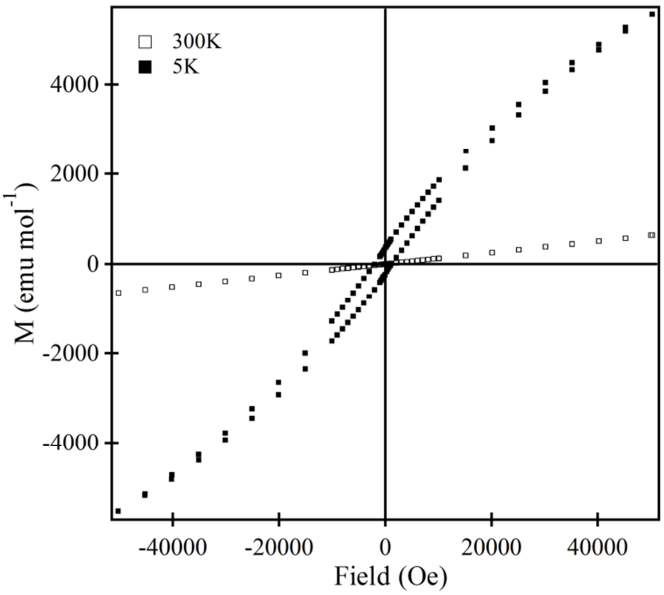

Figure S3. Magnetisation data collected as a function of applied field from $LaSr_3NiRuO_8$.

4. Topochemical reduction of $LaSr_3NiRuO_8$ with CaH_2.

Topochemical reduction of $LaSr_3NiRuO_8$ was performed using CaH_2 as a solid-state reducing agent. Small scale test reactions were performed by mixing ~300 mg of $LaSr_3NiRuO_8$ with 8 mole equivalents of CaH_2 in an argon-filled glove box. The mixtures were then sealed under vacuum in silica ampoules and then heated for two day periods in the range 300 – 500 ºC.

X-ray powder diffraction data indicated that at temperatures below 350 ºC there was no reaction. Heating at 400 ºC lead to the conversion of $LaSr_3NiRuO_8$ into a body-centred orthorhombic phase (a = 3.907 Å, b = 3.789 Å, c = 12.689 Å) determined by thermogravimetric reoxidation to be $LaSr_3NiRuO_7$. Raising the temperature to 425 ºC led to further reaction to form another body-centred orthorhombic phase (a = 3.853 Å, b = 3.593 Å, c = 13.011 Å) determined by thermogravimetric reoxidation to be $LaSr_3NiRuO_6$. Raising the temperature to 450 ºC led to a final reaction to from a body-centred tetragonal phase (a = 3.622 Å, c = 13.317 Å) which will be shown to be $LaSrNiRuO_4H_4$. Reactions performed at temperatures above 450 ºC led to decomposition to form Ni, Ru, La_2O_3 and SrO.

5. Preparation of $LaSr_3NiRuO_4H_4$

A sample of $LaSr_3NiRuO_4H_4$ suitable for analysis by neutron powder diffraction was prepared by grinding together approximately 1.5 g of $LaSr_3NiRuO_8$ with 0.4 g of CaH_2 in an argon filled glovebox using an agate mortar and pestle. The resulting powders were sealed in a silica ampoule and heated at 450 °C for 3 periods of 7 days, with the sample being reground between heating periods. Once the reaction was deemed complete, the reaction mixture was washed, under nitrogen, with 8 × 25 ml of 0.1 M solution of NH_4Cl in methanol in order to remove the CaO formed as a by-product of the reaction and any unreacted CaH_2. This was then followed by washing with 5 × 25 ml of clean methanol to dissolve NH_4Cl residues. The sample was then dried under vacuum.

6. Structural and chemical characterization of $LaSr_3NiRuO_4H_4$.

Time-of-flight neutron powder diffraction data (WISH, ISIS) collected from $LaSr_3NiRuO_4H_4$ could be indexed using a body-centred tetragonal unit cell with lattice parameters *a* = 3.6226(2) Å, *c* = 13.317(1) Å. A model based on the structure of $LaSr_3NiRuO_8$ was refined against the data but gave a poor fit until the occupancies of the anion sites were refined. It was observed that the 'equatorial' anion site occupancy rapidly refined to a negative value, indicating the presence of hydrogen at this position (H^1 neutron scattering length = -3.73 fm). Once the atom on this site had been changed to a hydride ion, the occupancy refined to unity, within error, confirming the stoichiometry of the phase as $LaSr_3NiRuO_4H_4$. Close inspection of the data revealed weak diffraction features corresponding to a small amount of CaO which had not been removed during the washing procedure, so this was added to the model as a second phase. Contributions from a very small quantity of an unidentified cubic impurity phase (*a* = 8.25 Å) were also observed in the data, but these were too weak to model. The refinement converged smoothly to give a good statistical fit (χ^2 = 3.855), and it was possible to refine anisotropic displacement ellipsoids for all atoms. The refined structural parameters are detailed in Tables S3 and S4, with a plot of the observed and calculated data shown in Figure S4.

	x	*y*	*z*	Fraction	U_{iso} equiv.(Å^2)
La/Sr(1)	0	0	0.3528(1)	0.25/0.75	0.011
Ni/Ru(1)	0	0	0	0.5/0.5	0.034
O(1)	0	0	0.1658(2)	1	0.027
H(1)	½	0	0	1	0.069
$LaSr_3NiRuO_4H_4$ space group *I*4/*mmm* (#139) Formula weight : 629.57 g mol^{-1}, Z = 2 Mass fraction: 97.3(2)% *a* = 3.6226(2) Å, *c* = 13.317(1) Å, Volume = 174.77(4) Å^3					
CaO space group *Fm*-3*m* (#225) Formula weight : 56.07 g mol^{-1}, Z = 4 Mass fraction: 2.7(2)% *a* = 4.8129(4) Å, Volume = 111.48(2) Å^3					
Radiation source: Neutron time of flight Temperature: 298 K χ^2 = 3.855; *wRp*= 1.78 %; *Rp* = 1.36 %.					

Table S3. Structural parameters from the refinement of $LaSr_3NiRuO_4H_4$ against neutron powder diffraction data collected at 300 K.

	U_{11}	U_{22}	U_{33}
La/Sr(1)	0.0068(11)	0.0068(11)	0.0194(25)
Ni/Ru(1)	0.0333(16)	0.0333(16)	0.0354(37)
O(1)	0.0205(10)	0.0205(10)	0.0409(23)
H(1)	0.0595(33)	0.0899(32)	0.0584(31)

Table S4. Anisotropic displacement factors from the structural the refinement of $LaSr_3NiRuO_4H_4$ against neutron powder diffraction data collected at 300 K.

Cation	Anion	length (Å)
La/Sr(1)	O(1)	2.490(3) × 1
	O(1)	2.574(1) × 4
	H(1)	2.669(1) × 4
Ni/Ru(1)	O(1)	2.208(3) × 2
	H(1)	1.811(1) × 4

Table S5. Selected bond lengths from the refined structure of $LaSr_3NiRuO_4H_4$.

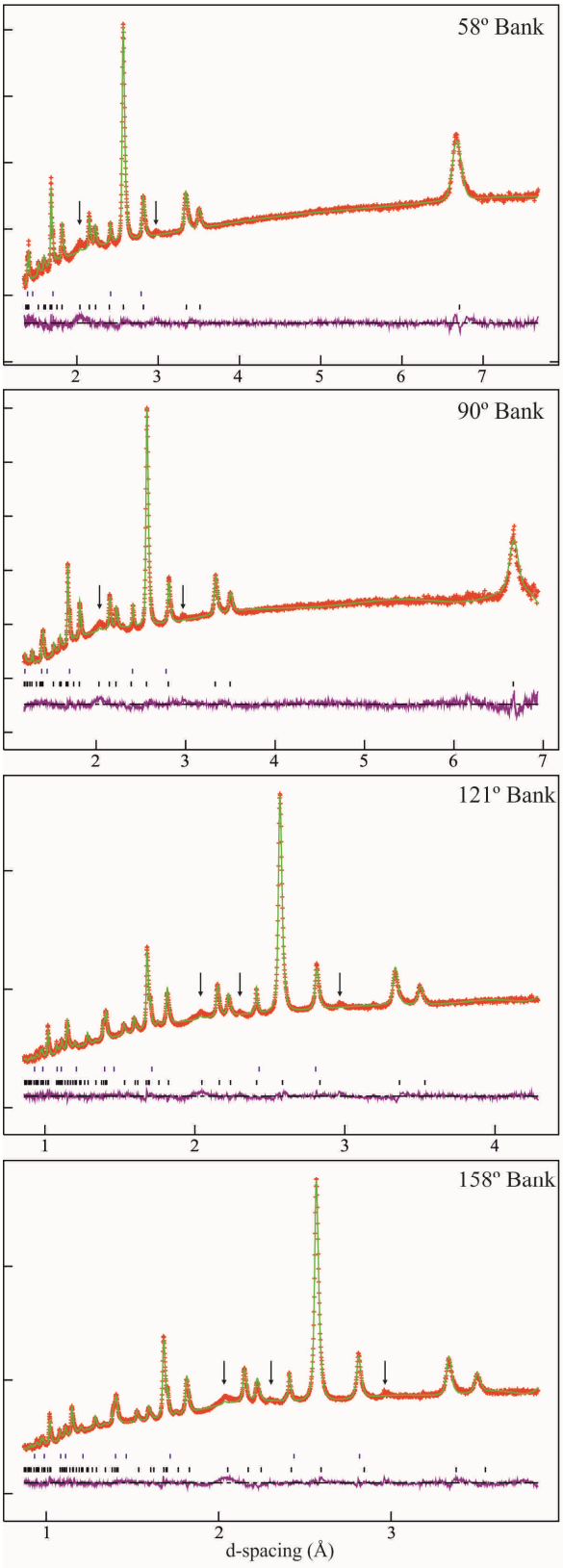

Figure S4. Observed calculated and difference plots from the refinement of $LaSr_3NiRuO_4H_4$ against neutron powder diffraction data collected at 300 K. Lower tick marks indicate peak positions of the majority phase, upper tick marks CaO. Arrows marks a series of weak reflections which can be indexed using a cubic cell, *a* = 8.25 Å, due to an unidentified impurity phase

7. Magnetic characterization of $LaSr_3NiRuO_4H_4$

Procedure used to measure the magnetization of samples containing elemental nickel:

The magnetization of elemental nickel is observed to saturate in applied magnetic fields of more than 2 T. Thus the paramagnetic susceptibility of a bulk sample can be measured in the presence of elemental nickel impurities by measuring the gradient of magnetization-field isotherms in applied fields larger than 2 T. As shown in Figure S5.

To this end the magnetization of samples was measured in a series of 7 fields between 2 T and 5 T, using a Quantum Design SQUID magnetometer. The magnetization vs. field data were fitted to a linear function, the gradient of which is the paramagnetic susceptibility of the bulk sample and the intercept is the saturated ferromagnetic moment of the sample. Data points with large errors were excluded from fits. All fits had at least 5 data points. This procedure was repeated at 5 K intervals between 5 K and 300 K to measure the temperature dependent susceptibility of samples.

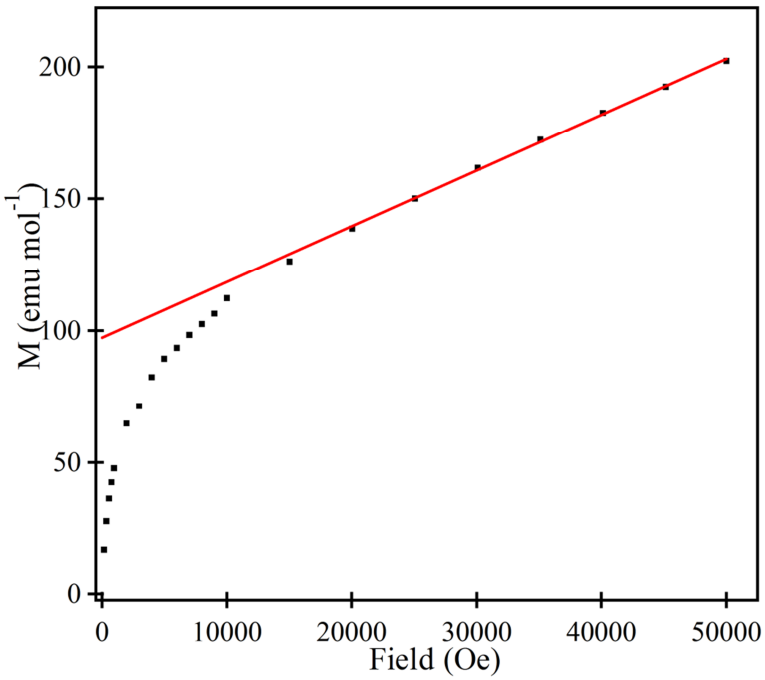

Figure S5. Magnetisation of a $LaSr_3NiRuO_4H_4$ sample measured as a function of applied field at 300 K. A linear fit to high-field region (H > 20000 Oe) yields a gradient which is the paramagnetic susceptibility of the sample, and an intercept which is the saturated ferromagnetic moment of the sample.

8. μ^+SR experimental details

The μ^+SR experiments were carried out at the Swiss Muon Source, PSI, Switzerland. In a μ^+SR experiment, spin-polarised muons were implanted in the bulk of a material and the time-dependence of their polarisation monitored by recording the angular distribution of the subsequent positron decay.

9. Computational details

All density functional calculations were performed using the VASP software package (VASP 5.3). The PBE functional was used, along with Hubbard *U* values (U_{eff}) of 6.0 eV on Ni and 3.0 eV on Ru to describe the effect of strong correlations. A plane-wave cutoff of 600 eV was imposed in all cases, and the Brillouin zone was sampled on a 5 × 5 × 3 *Γ*-centered grid. A 2√2 x 2√2 x 1 expansion of the primitive unit cell was used (Figure S6), which contains eight formula units. Neither the transition metal ions (Ni^{1+}/Ru^{2+}) nor the type-A cations (Sr^{2+}/La^{3+}) are distinguished by the modelling of the crystallographic data. We have therefore chosen to impose chequerboard order on the Ni/Ru layer: *i.e*. each Ru is surrounded by four Ni and *vice versa*, and the positions of Ni and Ru alternate along the *c* axis. The eight La^{3+} ions in the 2√2 x 2√2 x 1 expanded cell were positioned such that the distances between them are maximised. Several alternative arrangements were tested, with minimal impact on the lattice parameters or the projected density of states (DOS). The DOS shown in Figure 1 corresponds to a magnetic configuration where all Ni^{1+} spins are parallel within a Ni/RuH_2 layer, but alternate layers are antiferromagnetically aligned (shown by the red arrows in Figure S6). The DOS for a completely ferromagnetic arrangement was essentially identical. We were unable to converge to a configuration where the spins on Ni^{1+} are aligned anti-parallel to each other – this probably reflects the weak coupling between next nearest-neighbour Ni^{1+} ions *via* the intervening RuH_4 units. Optimized lattice parameters from the calculations are *a* = 3.637 Å, *c* = 13.418 Å compared to crystallographic values of *a* = 3.6226 Å and *c* = 13.317 Å, respectively.

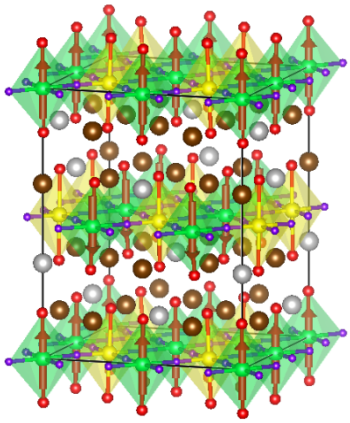

Figure S6. 2√2 x 2√2 x 1 expanded unit cell used in the computational model. Grey: La; Brown: Sr; Green: Ni; Yellow: Ru; Red: O; Purple: H.

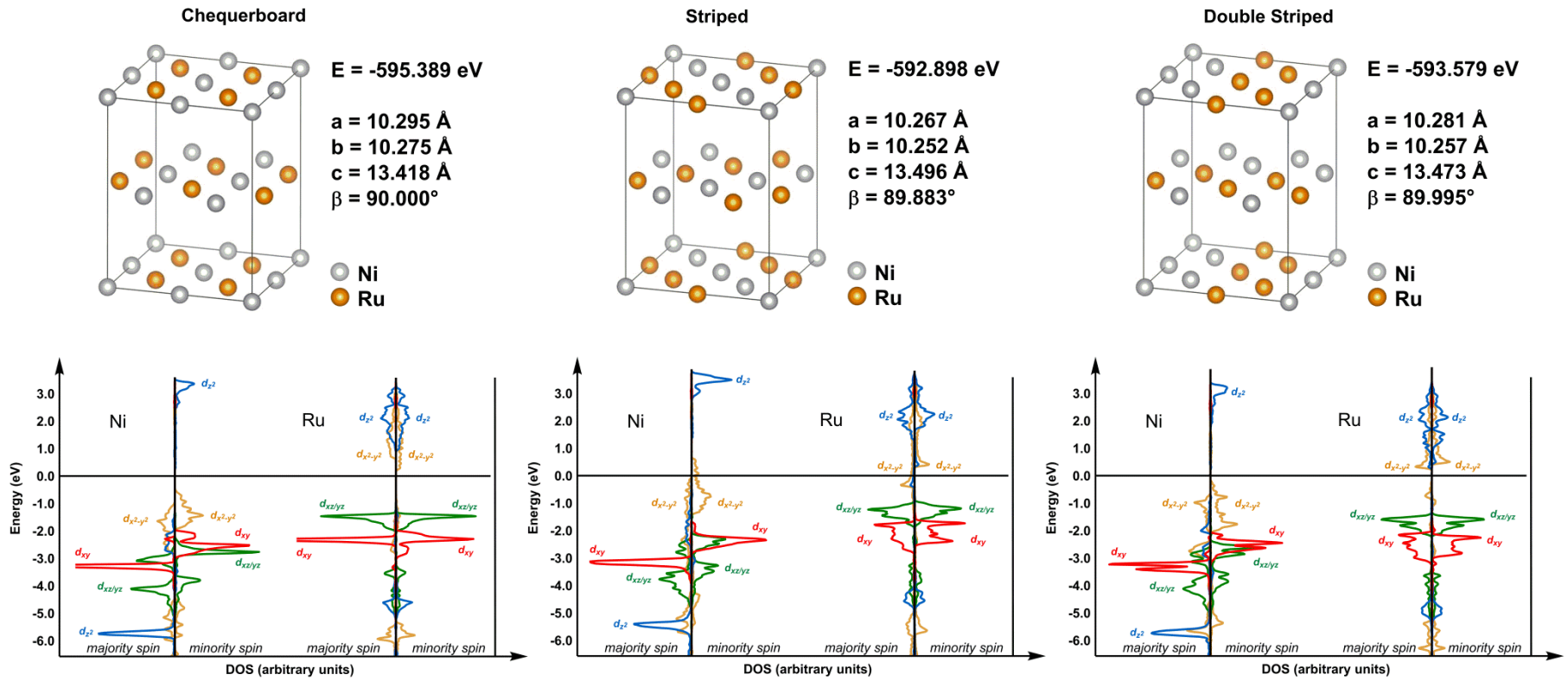

Figure S7. Structures, total energies and Ni/Ru DOS for the chequerboard, striped and double-striped arrangements of Ni/Ru in the unit cell.

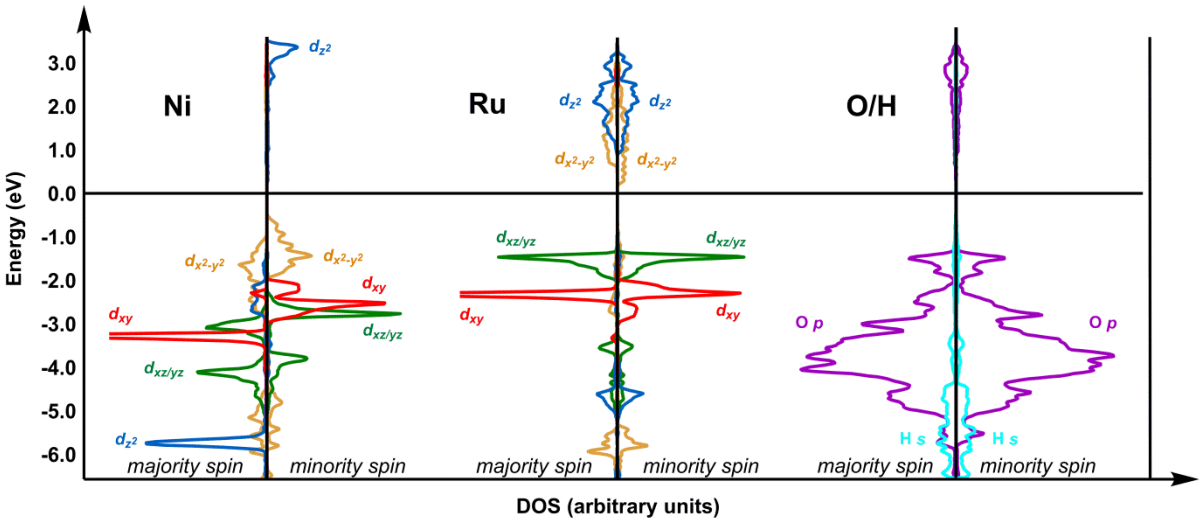

Figure S8. DOS for the chequerboard structure, including H^- and O^{2-} DOS as well as Ru and Ni.